Experimental Thermal and Fluid Science 151 (2024) 111073

Contents lists available at ScienceDirect

Experimental Thermal and Fluid Science

journal homepage: www.elsevier.com/locate/etfs

Experimental analysis of pulsatile flow effects on flow structure in transitional-type cavity

Justas Šereika *, Paulius Vilkinis, Gediminas Skarbalius, Algis Džiugys, Nerijus Pedišius

Laboratory of Heat-Equipment Research and Testing, Lithuanian Energy Institute, Breslaujos str. 3 Kaunas, LT-44403, Lithuania

ARTICLE INFO

Keywords:
Pulsatile flow
Flow separation
Transitional-type cavity
Turbulence intensity
Flow stability

ABSTRACT

Studies combining flow separation and pulsatile flow phenomena are inherent in the field of biomedicine and have many engineering and biomedical applications. In this study, the pulsatile flow structure is investigated experimentally based on a transitional-type cavity with a length-to-depth ratio of 8 using a microparticle image velocimetry system. A pulsatile flow is generated by pulsating the inlet pressure in sinusoidal pulses using a pressure control unit. Stationary flow and four sets of pulsatile parameters are investigated: two pulsation amplitudes (A = 0.15 and 0.60) and two pulsation frequencies (f = 0.5 and 1 Hz) in the Reynolds range of 50–2000. The recirculation flow dynamics in a cavity are analyzed by investigating the effect of pulsations on the flow structure and statistical flow parameters such as vorticity, shear rate, and turbulence intensity. The analysis shows that the effect of the pulsation amplitude on the recirculation zone dynamics is more prominent than that of the pulsation frequency. The magnitude of the recirculation zone reduction achieved by the pulsatile flow is inversely proportional to the pulsation amplitude. A reduction in the recirculation zone length decreases the shear rate distribution along the cavity. Additionally, an analysis into the turbulence intensity shows that effect of pulsations is negligible when the flow approaches the turbulent flow regime.

1. Introduction

Flow separation in channels with abrupt cross-sectional changes is inherent in many engineering applications, such as flows around vehicles, buildings, airfoils, and spoiler flows [1]. This phenomenon is typically encountered in general flow dynamics, heat transfer enhancement, particle trapping, and similar research fields [2–5]. The combination of flow separation and pulsatile flow is typically adopted in the biomedical field, e.g., in the blood flow in arteries, which is dominated by unsteady flow [6–8]. Furthermore, pulsatile flow in various lab-on-chip devices is receiving significant interest because they are adopted frequently in many engineering and biomedical applications [9,10]. Therefore, knowledge regarding pulsatile flow dynamics is a prerequisite for designing efficient applications.

When pulsations are applied to a flow, certain changes occur in the flow structure, which may alter its performance. Studies have shown that, owing to changes in the boundary layer and enhanced mixing in the separated shear layer, heat transfer is enhanced in flows over various channels [11–13] and cavity-like geometries [14–16]. Owing to the fundamental geometrical similarities and characteristics of blood flow, many pulsatile flow studies involving channels with abrupt cross-sectional changes have been performed to facilitate the mitigation of blood flow over plaques caused by stenosis. Studies have revealed that the stenosis increased the turbulence intensity [17], wall shear stress, and pressure drop on channel walls, thus resulting in the formation of chaotic fluid fields and unique vortical structures [17–19].

Several detailed investigations pertaining to separated flow dynamics in cavities have been performed to understand the underlying hydrodynamics. The separated flow is unsteady and presents global instabilities within the cavity, thus resulting in density and pressure fluctuations [20,21]. Chung et al. [22] showed that maximum fluctuations occurred in a transitional-type cavity owing to a sufficiently large downstream region and a sufficiently close rear edge of the cavity. In addition, an investigation into the shear layer structure in the cavity revealed that the cavity oscillations were sinusoidal in shape [23]. Considering the various flow structure investigations, many studies have been conducted on open- and closed-type cavities. Fishler et al. [24] experimentally investigated the flow in microscale cylindrical cavities and determined the effects of the geometry and Reynolds number (Re) on the flow structure. Faure et al. [5,25] comprehensively investigated the flow structure in open-type cavities while emphasizing the

* Corresponding author.
E-mail address: justas.sereika@lei.lt (J. Šereika).

https://doi.org/10.1016/j.expthermflusci.2023.111073
Received 29 May 2023; Received in revised form 27 September 2023; Accepted 9 October 2023
Available online 10 October 2023

Nomenclature

L	Cavity length
b	Cavity width
h_1	Cavity depth
h	Channel inlet/outlet height
H	Height of the channel in the cavity cross-section,$H = (h + h_1)$
D_h	Hydraulic diameter,$D_h = \frac{2hb}{(h+b)}$
ER	Expansion ratio,$ER = \frac{H}{h_1}$
AR	Aspect ratio,$AR = \frac{b}{h}$
x_R	Length of the recirculation zone
S	Inlet surface area
u	Velocity,$u = \sqrt{u_x^2 + u_y^2}$
u_x	x-axis velocity
u_y	y-axis velocity
U	Mean inlet velocity,$U = \frac{Q}{S}$
u'	Velocity fluctuation
$\overline{u}$	Mean phase velocity
$u_{x.rms}$	Root mean square of x-axis velocity
U'	Mean phase flow fluctuation
Q	Volumetric flow rate
u_{max}	Maximum velocity
u_φ	Phase velocity
A	Pulsation amplitude,$A = \frac{p_{max}}{p_0}$
f	Pulsation frequency
p	Pressure
p_0	Mean inlet pressure
p_{max}	Maximum pressure of pulsation cycle
φ	Pulsation phase angle
ν	Kinematic viscosity
Re	Reynolds number,$Re = \frac{Q \times h_1 \times \rho}{S \times \mu}$
Wo	Womersley number,$Wo = \sqrt{\frac{f \times D_h^2}{\nu}}$
TI	Turbulence intensity
γ	Shear rate,$\gamma = \frac{\partial u_x}{\partial y} + \frac{\partial u_y}{\partial x}\ \gamma = \partial U/\partial y + \partial V/\partial x$
ω	Vorticity,$\omega = \frac{\partial u_x}{\partial y} - \frac{\partial u_y}{\partial x}$
t	Time
T	Time period,$T = \frac{1}{f}$
τ	Measurement time
μ	Dynamic viscosity
Q_0	Volumetric flow rate at the inlet section

instabilities in the flow. Shen et al. [4] investigated rectangular micro-cavities at a low Re and defined three different flow patterns–attached, separated, and transitional–based on the separated shear layer reattachment on the bottom wall of the channel.

Guo and Luo [26] highlighted the dependence of the flow structure on the depth-to-length ratio and visualized the transition between different cavity flow types. Zhang et al. [27] identified the cavity length-to-depth ratio threshold values at which transitions between different cavity flow types occurred. Vilkinis and Pedišius [28] analyzed the recirculation zone length dynamics in transitional and closed-type cavities and revealed their dependence on the cavity length-to-depth and expansion ratios. Henderson et al. [29] investigated a time-dependent flow structure in a transitional-type cavity at a subsonic flow velocity. During the cycle, dumbbell-like flow structure changes appear in the vortex system, which consists of an elongated primary vortex near the leading edge and a weakened small vortex near the trailing edge, which, at the end of the cycle, is absorbed by the primary vortex. A time-averaged flow pattern consists of a single elongated vortex at the leading edge, occupying most of the cavity, with reattachment to the bottom wall of the cavity. Coleman et al. [30] and Leonardi et al. [31] investigated turbulent flow in rectangular cavities, separated by square bars. In the case of a transitional-type cavity, flow is comprised of two opposite-rotating vortices, where a large recirculation region is located upstream and a small one near the forward-facing step.

Pulsatile flow in cavities affects vortical structures the most significantly. Vortex dynamics proceed through different stages compared with stationary flows. Zhang et al. [32] investigated the vortex dynamics inside a deep rectangular cavity and observed that a five-stage vortex evolution, namely generation, traveling, merging, stretching, and weakening, was affected by Re and Womersley number (Wo). An increase in Re caused the vortex evolution stages to occurred earlier, whereas an increase in Wo resulted in the opposite effect. Owing to vortical pattern changes over the pulsation cycle, the average stationary flow structure differed from the pulsatile flow structure [14], thus resulting in changes in the flow structure and a reduced recirculation zone length [33–35]. These changes affected the parameters of related phenomena, such as the location of enhanced heat transfer [36] or pressure distribution in stenosis [17]. Therefore, generalized regularities of pulsatile flow in benchmark geometries are required to accelerate the development and increase the efficiency of applications related to the investigated phenomena. Currently, flows in open-type cavities are primarily investigated, whereas investigations into longer cavities characterized by separated shear layer reattachment to the bottom cavity wall, which are vital to the aforementioned problems and applications, are scarce.

Previously [35], we investigated the recirculation zone dynamics in a closed-type cavity at different pulsation frequencies (1, 2 and 5 Hz) and a maximum amplitude of $A = 1$, where we emphasized the recirculation zone structure at different pulsation cycle phases. As the most significant pulsation influence was observed at low pulsation frequencies, we kept it that way in this work. Furthermore, we decided to extend our research by adding 2 amplitude cases, since it is known to have different effect on the recirculation zone dynamics [37,38]. Amplitude cases of $A = 0.15$ and 0.60 serve as interim points between already studied $A = 1$ and the stationary flow case and allows to define the dependency of pulsation influence magnitude on flow structure. Wide Re range (50–2000) was chosen to cover different flow regimes, since the recirculation zone flow dynamics are heavily dependent on them. In this study, we continue our investigation of pulsatile flow dynamics in cavities by focusing on the effects of pulsation parameters on the flow. The pulsatile flow in a transitional-type cavity is investigated to determine the effects of pulsations on the flow structure in the cavity and statistical flow parameters such as vorticity, shear rate, and turbulence intensity (TI). As the recirculation zone length is dependent on the investigated parameters, the obtained results may serve as a roadmap for the application requiring flow control strategies, as the changes in recirculation zone influences the pressure distribution, drag characteristics as well as heat transfer intensity. This study is concentrated on pulsatile flow within a transitional-type micro-cavity from a foundational perspective, prioritizing a comprehensive understanding over immediate practical applications. The importance of this research lies in the enrichment of fundamental knowledge, which is inherent in designing efficient microfluidic applications.

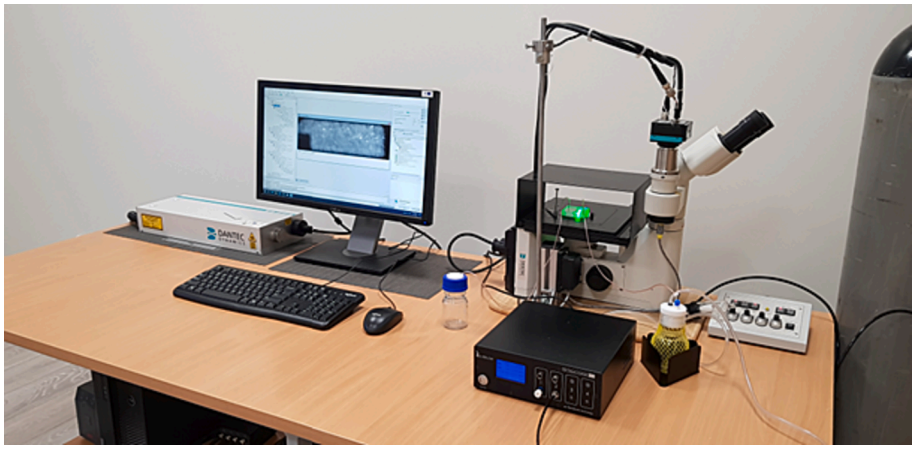

Fig. 1. Experimental facility.

2. Materials and methods

2.1. Experimental facility

In the current study, experiments were performed using the micro-particle image velocimetry (μPIV) method, which is based on monitoring the motion of tracer particles in a fluid. Deionized water with fluorescent particles measuring 1 μm in diameter was used as the working fluid. The specific gravity of the fluorescent particles was 1.05. The temperature was set to 21 ± 1 °C. The velocity components on the x- and y-axes were calculated based on the change in location of the seed particles and the measured time between image pairs.

The μPIV equipment (see Fig. 1) comprised an Elveflow OB1 MK3 pressure control unit (Elveflow, Paris, France), which generates inlet pressures up to 8 bar(g) in the experimental channel; Nd:YAG laser and its control unit; and a 4 Mpx FlowSense electro-optical charge-coupled device camera (Dantec Dynamics, Skovlunde, Denmark), which was mounted on Leica DM ILM inverted microscope (Leica Microsystems, Wetzlar, Germany). The matrix size of the camera was 7.4 μm, which resulted in a 1.5 mm × 1.6 mm field-of-view with 10x magnification. The laser and camera were synchronized to operate at a frequency of 15 Hz. The time between two sequent images was set to be between 1 and 500 μm based on the flow velocity. Time-averaged results were obtained by averaging 220 images. The fluorescent particle illumination light wavelength was equal to the laser-emitted light wavelength of 575 μm. The illuminated laser light was reflected by a dichroic mirror into a microchannel with immersed tracer particles. The immersed tracer particles emitted light, which was filtered by a dichroic mirror and recorded by a camera. The dichroic mirror permitted all light from one side, whereas it permitted only long-wavelength light from the other side. Consequently, all disruptive reflections were filtered.

The DynamicStudio v6.11 (Dantec Dynamics, Skovlunde, Denmark) and Octave v7.3.0 software was used to perform an analysis. The image pairs were analyzed using the adaptive particle image velocimetry method, which involves a grid predetermined based on the minimum and maximum windows sizes, where minimum and maximum interrogation windows measure 24 × 12 px and 64 × 24, respectively. The adjacent interrogation windows overlapped 25 % of the area, which resulted in a 25 μm gap between the x-axis velocity vectors and 20 μm between the y-axis velocity vectors. The correlation depth was 42.4 μm at a 10x magnification.

The velocity measurement uncertainty was evaluated by

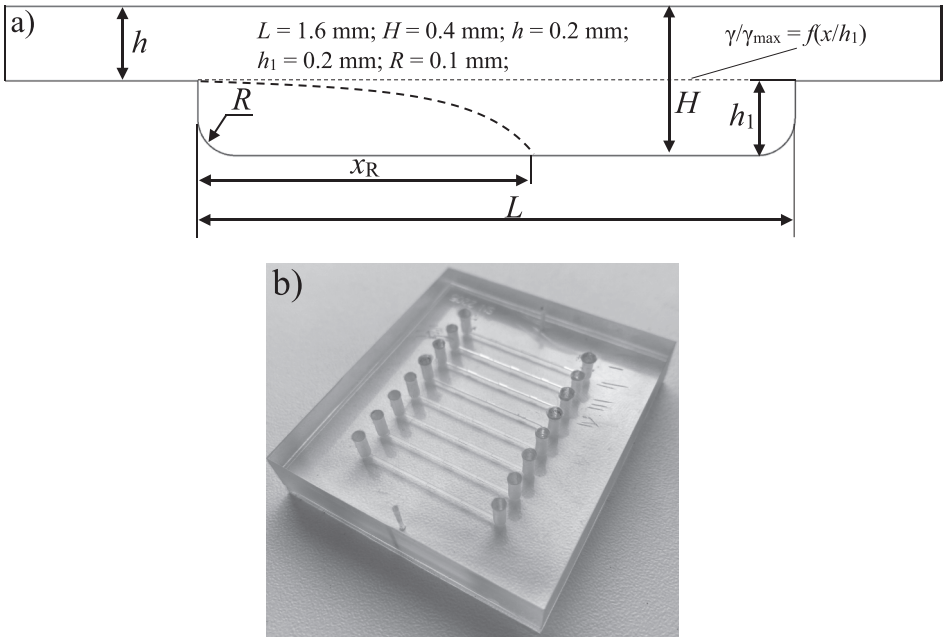

Fig. 2. (a) Schematic illustration and dimensions of the experimental channel; (b) image of the experimental microchannel chip.

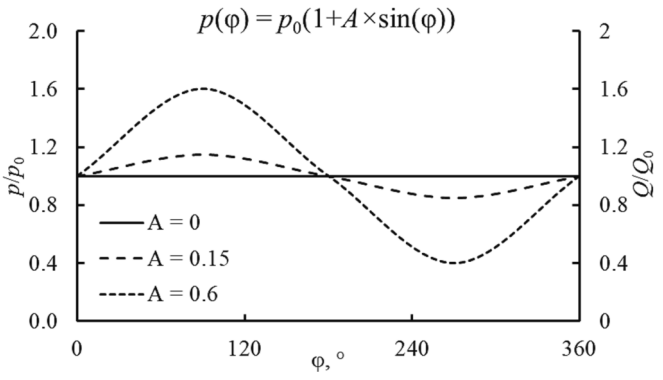

Fig. 3. Variation of pressure and volumetric flow rate at experimental channel inlet during pulsation cycle with different pulsation amplitudes.

Table 1
Amplitude and pulsation frequency of different flow cases.

Case	*Wo*	*A*	*f, Hz*
1	*0*	*–*	*–*
2	*0.21*	*0.15*	*0.5*
3	*0.30*	*0.15*	*1.0*
4	*0.21*	*0.60*	*0.5*
5	*0.30*	*0.60*	*1.0*

determining the contribution of the expanded uncertainty of the flow generated by the pressure control unit (≤0.5 %), experimental channel dimensions (≤3 %), uncertainty in the correlation calculation owing to its dependence on the selected time difference between image pairs (≤0.5 %), and uncertainty in the velocity measurement repeatability (≤2 %). The expanded uncertainty of velocity measurement by the μPIV equipment did not exceed 7 %.

There are three main components of uncertainty for recirculation zone length. The exact reattachment location could not be determined owing to the limited spatial resolution of μPIV. Moreover, to obtain images with a high spatial resolution and low measurement depth, high-magnification objective lenses were used. Therefore, the field of view becomes extremely small to cover the entire cavity at once, and images of separate parts of the cavity were taken and combined. Recirculation zone length was determined according to the location where the reattached flow split into the upstream and downstream flows. This location slightly changes over time; therefore, the reattachment point was determined for every image pair. This variation was minimal in the laminar flow regime, and the repeatability did not exceed 2.3 %. In the turbulent flow regime, the reattachment point fluctuated more and repeatability reached 8.9 %. The total expanded uncertainty of the reattachment point evaluation did not exceed 15 %.

2.2. Physical object

In this study, experiments were performed in a transitional-type microcavity with a length-to-depth ratio of $L/h_1 = 8$. The expansion and aspect ratios of the channel were ER = 2 and AR = 3, respectively. A schematic illustration and the image of the experimental channel are shown in Fig. 2. The microchannel chip was manufactured in polycarbonate using CNC machining (Fig. 2b). The channel with cavities was cut in a lower plate and then covered with plate with inlet and outer ports and glued together. The thickness of lower and upper plates was 10 mm and 2 mm, respectively. The microchannel chip consists of 8 separate channels with identical geometries. The channel length is ~ 4 cm. The inlet length was set to 20 hydraulic diameters. The experiments were performed in the Re range of $50 < Re < 2000$ under stationary and pulsatile flow conditions. For the Re calculations, the velocity was obtained from the measured volumetric flow rate values at different inlet pressure points; subsequently, a dependency curve from which Re was obtained using the interpolation method was constructed. The volumetric flow rate was measured by using a measuring cylinder with volume of 25 ± 0.25 ml and a chronometer. A pulsatile flow was achieved by pulsating the pressure at the inlet with sinusoidal pulses. The graph in Fig. 3 shows the variation in the inlet pressure during the pulsation cycle. Table 1 lists the pulsation amplitude and frequency values for the different flow cases. Case 1 corresponds to the stationary flow case; therefore, its pulsation amplitude and frequency are not provided.

2.3. Recirculation zone length measurements

The recirculation zone length was determined by measuring the u_x values at the lowest possible y position. The separated shear layer reattachment point is located where the x-axis velocity vectors change direction.

2.4. Turbulence intensity and phase velocity calculations

Due to pulsating nature of the inlet, flow inside measurement area pulsates with the period $T = 1/f$. Measurements were made with time step $\Delta t = 0.067$ s. Number of snapshots were $N = 180 or 210$, depending on pulsation frequency, number of snapshots during one period $n = T/\Delta t$. Number of pulsations periods during all measurement time is $N_T = N/n$.

In order to estimate turbulent properties of the flow, we should separate the mean phase flow and fluctuations. The mean phase flow velocity is characterized by periodicity in every period of pulsation:

$$\overline{u}(\tau + kT) = \overline{u}(\tau), k = [0, N_T - 1] \tag{1}$$

Accordingly, measured velocity in each point at each measurement time can be separated into the components of pulsating (mean phase flow) velocity $\overline{u}$ and fluctuating velocity u':

$$u(t_i) = \overline{u}(t_i) + u'(t_i) \tag{2}$$

where i is time index of measurement:

$$t_i = i\Delta t, i = [0, N - 1] \tag{3}$$

where Δt is the time difference between two consecutive snapshots. The mean phase flow velocity is estimated as follows:

$$\overline{u}(\tau_j) = \frac{\sum_{i=0}^{N-1} u(t_i)\delta(\tau_j, mod(t_i, T))}{\sum_{i=0}^{N-1} \delta(\tau_j, mod(t_i, T))}, \tau_j = j\Delta t, j = [0, n]. \tag{4}$$

where δ is defined as:

$$\delta(x, y) = \begin{cases} 0, if x \neq y \\ 1, if x = y \end{cases} \tag{5}$$

The mod function returns the remainder of the division.

Additionally, outlier velocity points were removed from temporal data at a confidence interval of 95 % from mean phase velocity. The average velocity of the mean phase flow velocity is estimated as follows:

$$\langle \overline{u} \rangle = \frac{1}{n} \sum_{j=0}^{n} \overline{u}(\tau_j), \tau_j = j\Delta t, j = [0, n] \tag{6}$$

Turbulent energy *TKE* at each phase time was estimated as follows:

$$TKE(\tau_j) = \frac{3}{4} \frac{\sum_{i=0}^{N-1} \left(u_x'^2(t_i) + u_y'^2(t_i) \right) \delta(\tau_j, mod(t_i, T))}{\sum_{i=0}^{N-1} \delta(\tau_j, mod(t_i, T))}, \tau_j = j\Delta t, j = [0, n] \tag{7}$$

Finally, turbulent intensity *TI* was estimated as follows:

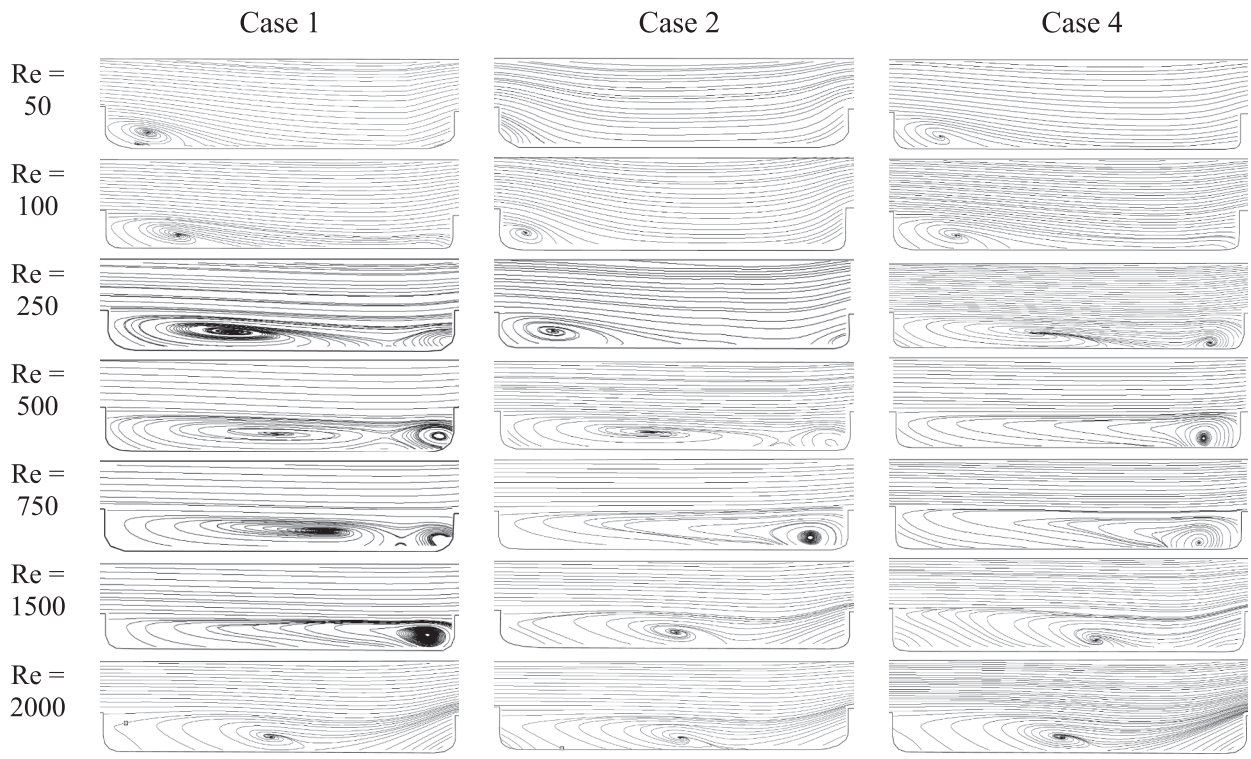

Fig. 4. Time-averaged velocity streamlines at Re = 50–2000 for Cases 1, 2, and 4.

$$TI(\tau_j) = \frac{U'(\tau_j)}{U} = \frac{\sqrt{\frac{2}{3}TKE(\tau_j)}}{U}, \tau_j = j\Delta t, j = [0, n] \quad (8)$$

Averaged turbulent intensity was defined as:

$$\langle TI \rangle = \frac{1}{n}\sum_{j=0}^{n} TI(\tau_j), \tau_j = j\Delta t, j = [0, n] \quad (9)$$

3. Results and discussion

3.1. Flow structure analysis

The velocity streamlines at various Re values and different flow cases were analyzed to determine the dynamics of the recirculation zone in the cavity based on the flow regime, pulsation amplitude, and frequency. Velocity streamlines given in Fig. 4 were obtained by averaging the flow images during a 14.6 s flow, which corresponded to 220 image pairs at a camera frequency of 15 Hz. The flow structure dependence on the pulsation frequency in the investigated frequency range was insignificant, and the flow fields of Cases 2 and 4 were consistent with those of Cases 3 and 5, respectively. Therefore, in Fig. 4, only the flow fields in cases with different amplitude values (Cases 2 and 4) are presented. At Re = 50, the recirculation zone length was altered, or the recirculation zone completely disappeared when pulsations were applied. The recirculation zone length reduced under pulsatile flow conditions at Re = 100–250 (Fig. 4). In a transitional-type cavity, the beginning of the transitional flow regime is determined by the formation of a stagnant recirculation zone without shear layer reattachment. A transition to the turbulent flow regime occurs when the separated shear layer is attached to the cavity bottom [28]. The transitions to different flow regimes can be seen in Fig. 6. In all the pulsatile flow cases, the transitional flow regime is achieved in Re range of Re = 250–1250. In the transitional flow regime at Re = 500–750, the shear layer remained detached from the cavity bottom in the pulsatile flow in all investigated cases; however, changes in the location of the vortex core and vortex size were observed. At Re = 1250, the separated shear layer reattached to the bottom of the cavity when pulsations were applied, which resulted in an earlier transition to the turbulent flow regime compared to the stationary flow. At the beginning of the turbulent flow regime, when Re > 1750, the effect of the flow pulsations diminished because no apparent changes in the flow structure were observed in the investigated cases.

During the pulsation cycle, the dynamics of the recirculation zone depend on the flow regime. Fig. 5 shows the instantaneous flow velocity streamlines for different phases of the pulsation cycle. In the laminar flow regime (Re = 100), the variation in velocity during the pulsation cycle influences the length of the recirculation zone, causing it to increase and decrease depending on the phase of the cycle. It is important to note that the recirculation zone's dependency on Re in the laminar flow regime follows a nearly linear relationship. Consequently, during the cycle, the recirculation zone length increases during velocity forcing phase (at $0° < \varphi < 90°$ and $270° < \varphi < 360°$) and decreases during flow deceleration phase (at $90° < \varphi < 270°$). Pulsatile flow causes the vortex center to change its position, but the recirculation zone remains present.

In the transitional flow regime, a different mechanism governs the development of the recirculation zone. It is no longer stagnant and comprises periodically recurring vortices, as previously discussed by Vilkinis and Pedišius [28]. In Fig. 5, at Re = 1000, these recurring vortices are observable throughout the pulsation cycle. A prominent vortex emerges behind the BFS and dissipates while traveling towards the FFS. Interestingly, at certain moments of the pulsation cycle, two vortex cores are observed, with the second one dissipating only after the occurrence of the first. The recurring vortices traverse the entire cavity, resulting the separated shear layer to remain unattached to the bottom of the cavity throughout the entire pulsation cycle. The same mechanism applies to Re = 2000, although vortex movement is more chaotic. At certain pulsation phases, three vortex cores are observed, indicating that the frequency of recurring vortices is higher compared to pulsatile flow at Re = 1000.

The other investigated pulsatile flow cases show similar tendencies where the frequency of recurring vortices corelate with the pulsation parameters and determine the recirculation zone length.

The recirculation zone length dependency on Re given in Fig. 6 are

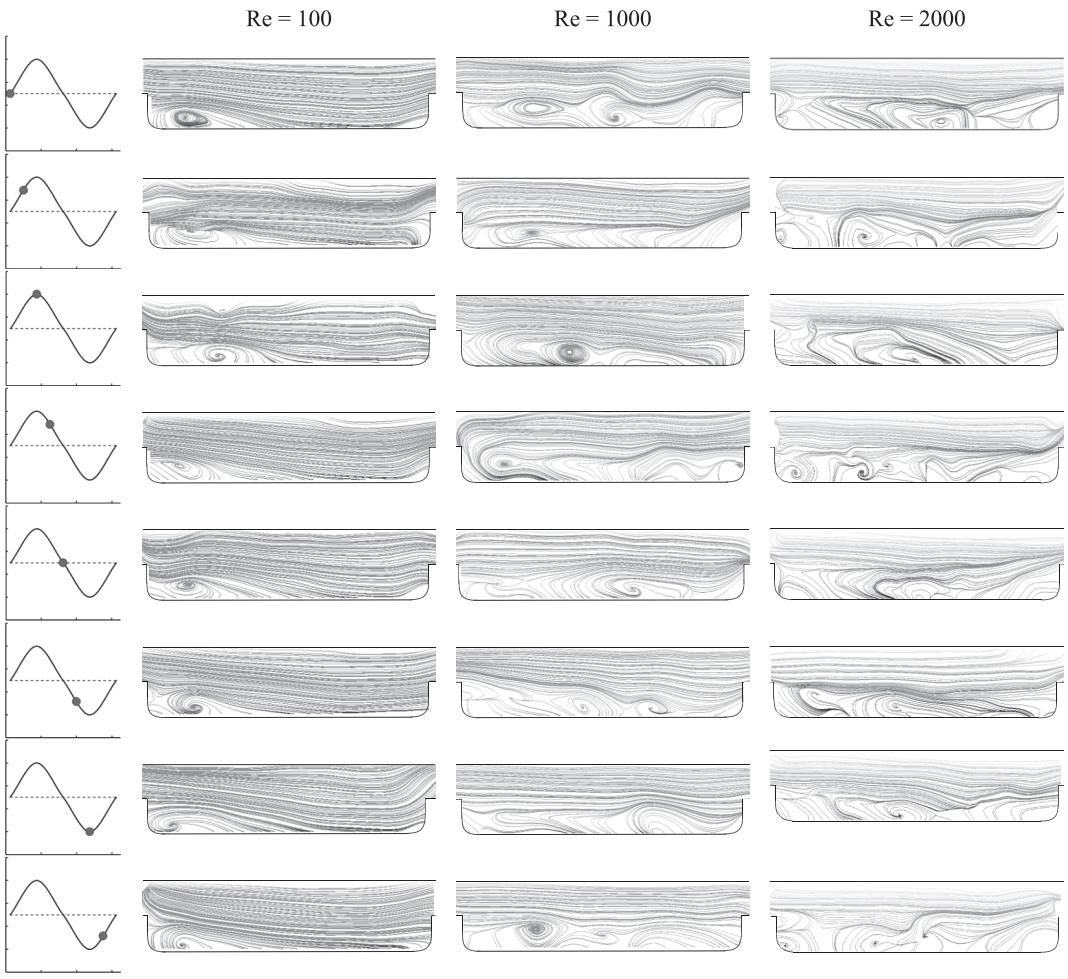

Fig. 5. Flow velocity streamline variation during the pulsation cycle at Re = 100 – 2000 of Case 4.

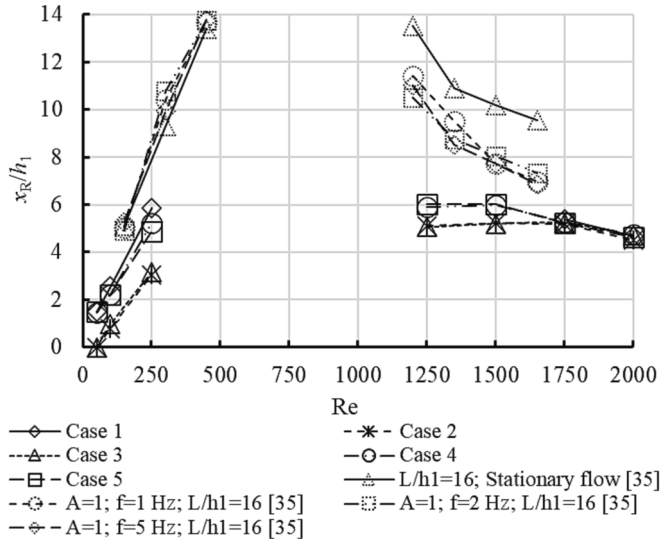

Fig. 6. Time-averaged recirculation zone length dependence on Re.

obtained using the same approach as in Fig. 4, where the flow is averaged throughout the whole measurement. The changes of the recirculation zone length depended on the pulsation amplitude. Lower recirculation zone length values observed in pulsatile flow Cases 2–5 at Re = 50–250 were caused by small vortices in the separated shear layer [39], which increased the shear layer growth rate and decreased the recirculation zone length. The reduction in the recirculation zone length at A = 0.15 was determined based on the linear recirculation zone length growth in the laminar flow regime and the significant change in its structure in the transitional flow regime. When the pulsation amplitude was low (A = 0.15), the flow remained primarily in the same flow regime, and changes in the recirculation zone size remained linear during the flow pulsation cycle. When the pulsation amplitude was high (A = 0.6), the velocity oscillated more significantly, and a transitional flow regime may be reached when the recirculation zone length increment during the positive phase is large. Therefore, time-averaged flow fields feature larger recirculation zone lengths in high-amplitude cases than in low-amplitude cases because the cavity is filled with a stagnant recirculation zone for a certain period. For the same reason, separated shear layer reattachment occurred at a lower Re compared with the case of stationary flow (Re = 1250 at pulsatile flow and Re = 1750 at stationary flow), and smaller recirculation zone lengths were observed at the beginning of the turbulent flow regime in the pulsatile flow cases. The same trend was observed in our previous work [35], where the recirculation zone reduction effect was observed at Re > 1200 in a closed-type cavity. However, the main difference between pulsatile flow effects in different types of cavities is observed in laminar flow, where pulsations with A = 1 show little to no effect on recirculation zone length. The discrepancies in laminar flow regime are marginal and do not exceed the measurement uncertainty. By comparing the results of two consequent studies, it is observed, that the recirculation zone reduction effect in laminar flow regime is inversely proportionate to pulsation amplitude, as the most significant effect is observed when A =

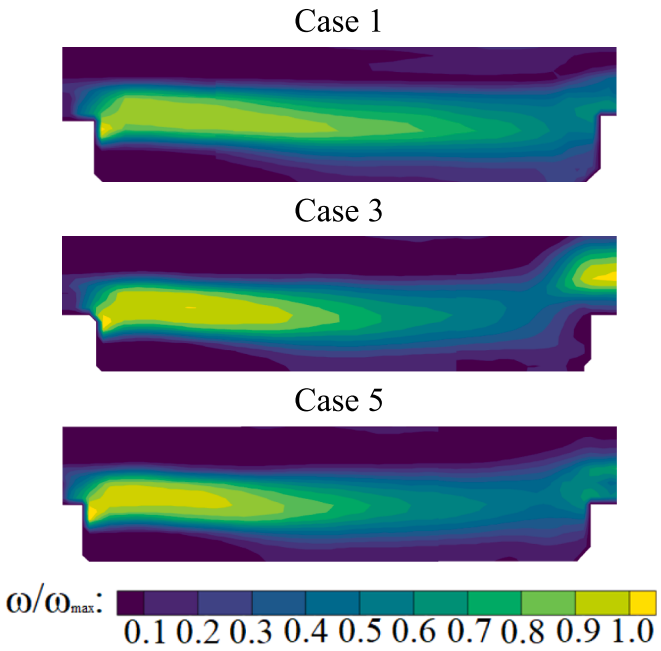

Fig. 7. Relative vorticity ω/ω_{max} contours of both stationary and pulsatile flow cases at Re = 1500.

0.15 and the least significant at A = 1. In laminar flow regime high amplitude pulsations (A = 1) introduce strong disturbances to the recirculation zone and the transitional-type cavity encloses it with a closely positioned FFS. This potentially leads to perturbed and extensive recirculation zone. Smaller amplitude pulsations (A = 0.15) lead to weaker recirculation zone disturbances; therefore, leading to more steady recirculation zone, which length is reduced due to the pulsatile flow impact on the vortices in the shear layer as mentioned earlier. This finding is only valid for transitional- and closed-type cavities as the absence of FFS in flow over BFS typically leads to larger variations of flow rate during the pulsation cycle and alter the recirculation zone differently [38].

In addition, the recirculation zone interacted with the vortex near the forward-facing step (FFS) in the transitional flow regime. Under pulsatile flow conditions, the interaction was more intense; therefore, the recirculation zone center location shifted to the FFS earlier compared with the stationary flow case. This effect was achieved earlier when A = 0.60, compared to cases with A = 0.15. When Re > 1750, the recirculation zone length no longer depends on Re and the pulsation parameters, which is the case for flows over cavities and backward-facing steps in turbulent flow regime [38,40,41].

Recirculation zone length reduction in pulsatile flow is characteristic of closed-type cavities and channels with BFSs [35,38], and the present results reveal that this phenomenon is achieved even if the flow is affected significantly by FFSs. The highest recirculation zone length reduction was achieved at the beginning of the transitional flow regime at Re = 250 and was estimated to be ~ 45 % and 17 % for low- and high amplitude cases, respectively, compared with the case of stationary flow. Conversely, the pulsation frequency was shown to have negligible effect on the recirculation zone length. It was observed that the discrepancies between cases with different frequency were less than 6 %, meaning that the recirculation zone length in Case 2 was almost identical to that in Case 3. The same observation was made in Cases 4 and 5. Nevertheless, the dynamic trend of the recirculation zone length in all pulsation cases remained the same as that of the stationary flow (Fig. 6).

3.2. Flow statistics

The relative vorticity contours are shown in Fig. 7. Since the relative vorticity contours in Cases 2 and 4 are consistent with those in Cases 3 and 5, respectively, only one pulsation amplitude case is presented. In all the cases, the highest vorticity was located in the separated shear layer and at the edge of the FFS. In pulsatile flow, the vorticity increased at these locations owing to increased vortex shedding. Higher vorticity values were indicated in the separated shear layer stretched downstream of the cavity. The separated shear layer tended to flap in the cavity [42–45], which is consistent with low-amplitude pulsations in the recirculation zone, thereby increasing the swirling motion. The vorticity increment in the shear layer was comparable for all the presented flow fields. However, the pulsatile flow influence on the vorticity near the FFS was more significant at a lower amplitude. The vortex formed behind the FFS was extruded from the cavity, resulting in a higher vorticity at the outlet. By contrast, during higher-amplitude pulsations,

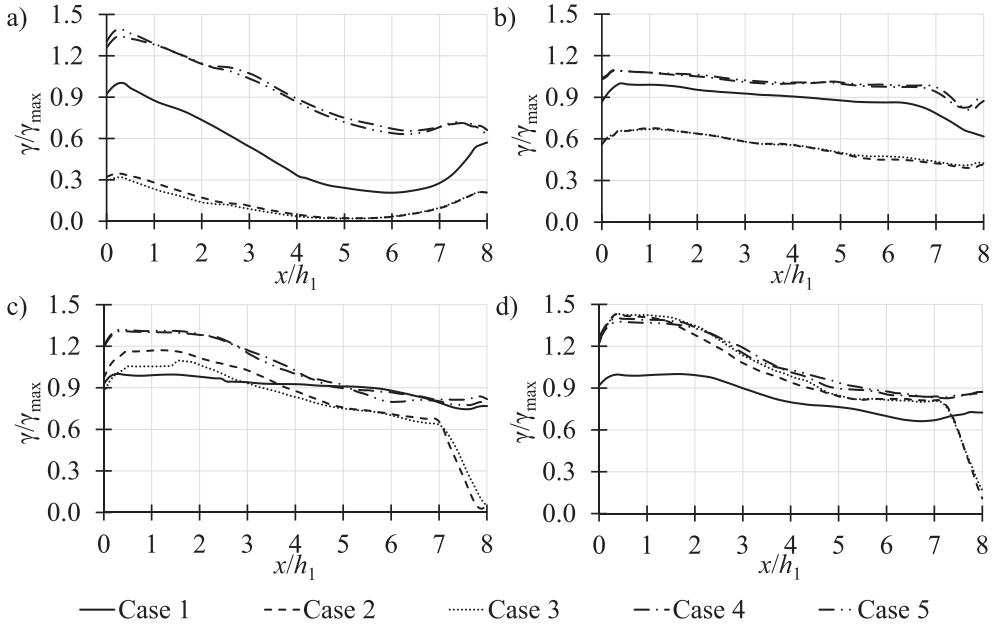

Fig. 8. Longitudinal shear rate profile along cavity at Re values of (a) 100, (b) 500, (c) 1500, and (d) 2000.

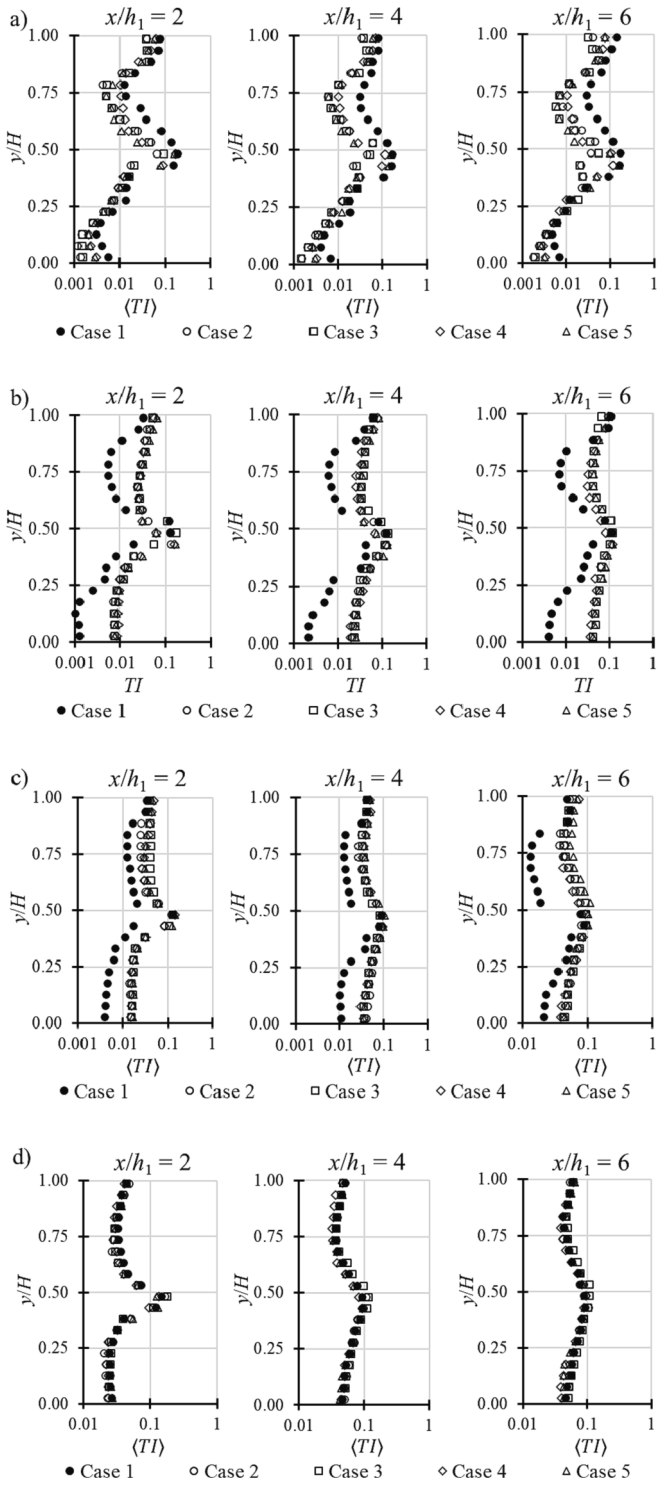

Fig. 9. ⟨*TI*⟩ profiles at Re values of (a) 500, (b) 1000, (c) 1500, and (d) 2000.

the vortex dissipated with the recirculation zone. The maximum values of vorticity differed depending on the pulsation amplitude. In stationary flow case (Case 1) maximum vorticity has reached 2.1×10^4, in Cases 2–3 – 2.3×10^4, and in cases 4–5 – 2.8×10^4. This 29 % increment of Cases 4–5, compared to stationary flow case, shows that increased velocity variation in higher amplitude cases causes magnified swirling motion in the shear layer, just above the recuring vortices, even though the general flow topology is not impacted.

The longitudinal shear-rate profiles in Fig. 8 represent fluid mixing in the separated shear layer. The profile locations are shown in Fig. 2a. For calculations of share rate, the mean phase flow and fluctuations were not separated. Parameter γ_{max} corresponds to the maximum shear rate value of the stationary flow case (Case 1). At Re = 100; 500; 1500; 2000 the $\gamma_{max} = 1.62 \times 10^3$; 1.08×10^4; 1.89×10^4; 2.47×10^4 respectively. The shear-rate distribution along the cavity depends on the structure of the recirculation zone, particularly its length. The longer the recirculation zone, the further the separated shear layer stretches above the cavity, thereby maintaining high shear rate values. The recirculation zone and separated shear layer at low Re are sensitive to flow pulsations. At high pulsation amplitudes, the recirculation zone is disrupted, causing increased instability in the flow, whereas at low amplitudes, the energy of the disturbances decreases [46]. Therefore, at Re = 100–500, the shear rate along the cavity decreased at low amplitudes and increased in high-amplitude cases compared with the case of stationary flow. At a higher Re (i.e., 1500), the shear rate in the stationary flow became constant along the cavity. In this case, the cavity was filled with a stagnant recirculation zone, which was disrupted during oscillations; therefore, the shear rate in the first section of the cavity ($x/h_1 > 4$) increased in the pulsatile flow. As Re increased further (Re = 2000), the differences between the different pulsatile flow cases diminished, and a higher shear rate was observed in the pulsatile flow.

At Re = 1500 and 2000, the relative shear rate decreased abruptly at $x/h_1 = 7$ in Cases 2 and 3. When the pulsation amplitude was low, the vortex near the FFS was extruded from the cavity, as shown in the momentary streamlines of pulsatile cycle given in Fig. 5. Subsequently, the separated shear layer attached to the bottom of the cavity, thus resulting in a lower shear rate at the measured location. In the high-amplitude cases (Cases 4 and 5), the flow structure in the cavity remained steady during the pulsation cycle. Therefore, no abrupt changes in the statistical flow data were observed.

The ⟨TI⟩ profiles at different cavity locations are shown in Fig. 9. It is known that an increase in the turbulence intensity causes instabilities and secondary flows [47]. In our previous study [35], we showed that pulsations increased the ⟨TI⟩ and might resonate with the flapping motion of the separated shear layer and recirculation zone, thus increasing instabilities in certain regions of the cavity.

At Re = 500, pulsations decreased ⟨TI⟩ in the main flow compared to stationary flow, due to presence of shear layer reattachment moments during the pulsation cycle when $\frac{u(t_i)}{\langle u(t_i)\rangle} < 1$ (at $180^\circ < \varphi < 360^\circ$). Additionally, at Re = 500, the flow was in the transitional regime, in which the velocity fluctuations increased; therefore, as the velocity decreased during the pulsation cycle, the flow re-entered the laminar regime and reduced the ⟨TI⟩ in all the pulsatile cases. As Re increased to 1000–2000, the ⟨TI⟩ dependency on the pulsatile parameters became less significant because the flow is starting to approach a turbulent regime, and the properties of additional disturbances become less relevant. In the cases of Re = 1000 and Re = 1500 (Fig. 9 b and c), the ⟨TI⟩ in all the pulsatile flow cases exceeded than that in the stationary flow. In the Re range of 1000—1500 and in the case of pulsatile flow, the recirculation zone length varied throughout the cavity, thereby generating more instabilities in the flow and higher ⟨TI⟩ values compared with the stationary flow. At Re = 2000 (Fig. 9 d), the velocity fluctuations caused by the turbulent flow regime became dominant; therefore, the instabilities caused by the pulsations were negligible, and a uniform distribution of ⟨TI⟩ was observed.

4. Conclusions

In this study, the flow structure in the transitional-type cavity with length-to-depth ratio $L/h_1 = 8$ was investigated under stationary and pulsatile flow conditions in a wide Re range Re = 50 – 2000. Two different pulsation amplitudes (A = 0.15 and 0.60) and frequencies (f = 0.5 and 1.0 Hz) were selected. The flow structure in the cavity, recirculation zone length dynamics, and flow statistical data such as vorticity, shear rate, and turbulent intensity were analysed depending

on pulsatile flow parameters and Re.

Analysis of recirculation zone length dynamics revealed that its length and structure depend on pulsation amplitude, whereas the pulsation frequency had only minor effects on it, as only marginal effects are observed between flow cases with the same pulsation frequency The recirculation zone length reduction is highest in the laminar flow regime. and it is inversely proportionate to pulsation amplitude. It reduces 45 % and 17 % at low (0.15) and high (0.6) amplitude cases respectively, compared to stationary flow. These finding are specific for transitional- and closed-type cavities as it depends on the presence of FFS.

In a turbulent flow regime, the influence of pulsatile flow parameters is insignificant as the recirculation zone length becomes independent of flow parameters. The transition to a turbulent flow regime occurs at lower Re in all pulsatile flow cases compared to stationary flow.

Vorticity increment in the pulsatile flow is observed in all cases at the separated shear layer and near FFS at low pulsation amplitude due to increased flow instabilities in the cavity. The shear rate distribution along the cavity indicates that high pulsation amplitude causes increased instabilities in the flow due to the breakdown of the recirculation zone, while the energy of disturbances decreases when the amplitude is low. When the cavity is filled with a stagnant recirculation zone (at Re = 1500), the shear rate is increased in the first part of the cavity ($x/h_1 > 4$) due to its breakdown during the oscillations.

Pulsatile flow causes the turbulence intensity reduction at Re = 500 as a consequence of the shorter reattached shear layer within the cavity. As Re increases to Re = 1000 – 2000, ⟨TI⟩ dependency on pulsatile parameters becomes less significant, since the flow leaves the laminar regime where the properties of additional disturbances are less relevant. Finally, at Re = 2000, the uniform ⟨TI⟩ distribution is observed from all the investigated cases, since the fluctuations caused by turbulent flow itself become dominant.

Funding

This study was funded by the Research Council of Lithuania (grant number S-MIP-21–21).

CRediT authorship contribution statement

Justas Šereika: Conceptualization, Validation, Investigation, Formal analysis. **Paulius Vilkinis:** Conceptualization, Investigation, Supervision. **Gediminas Skarbalius:** Validation, Investigation. **Algis Džiugys:** Validation, Investigation, Supervision. **Nerijus Pedišius:** Conceptualization, Resources, Project administration.

Declaration of Competing Interest

The authors declare that they have no known competing financial interests or personal relationships that could have appeared to influence the work reported in this paper.

Data availability

No data was used for the research described in the article.

References

[1] L. Chen, K. Asai, T. Nonomura, G. Xi, T. Liu, A review of Backward-Facing Step (BFS) flow mechanisms, heat transfer and control, Therm. Sci. Eng. Prog. 6 (2018) 194–216, https://doi.org/10.1016/j.tsep.2018.04.004.

[2] J. Wang, T. Ma, Z. Wang, R. Wang, H. Song, W. Yuan, H. Zheng, Three-dimensional flow structures and heat transfer characteristics of compressible flow over a cylindrical cavity, Aerosp. Sci. Technol. 122 (2022), https://doi.org/10.1016/j.ast.2022.107408.

[3] F. Shen, M. Xu, Z. Wang, Z.M. Liu, Single-particle trapping, orbiting, and rotating in a microcavity using microfluidics, Appl. Phys Express 10 (2017), https://doi.org/10.7567/APEX.10.097301.

[4] F. Shen, P. Xiao, Z. Liu, Microparticle image velocimetry (μPIV) study of microcavity flow at low Reynolds number, Microfluid Nanofluidics. 19 (2015) 403–417, https://doi.org/10.1007/s10404-015-1575-3.

[5] T.M. Faure, Velocity field and parametric analysis of a subsonic, medium-Reynolds number cavity flow, Exp. Fluids 55 (2014) 1822, https://doi.org/10.1007/s00348-014-1822-5.

[6] D.N. Ku, Blood flow in arteries, Annu. Rev. Fluid Mech. 29 (1997) 399–434, https://doi.org/10.1146/annurev.fluid.29.1.399.

[7] B. Sharifzadeh, R. Kalbasi, M. Jahangiri, D. Toghraie, A. Karimipour, Computer modeling of pulsatile blood flow in elastic artery using a software program for application in biomedical engineering, Comput. Methods Programs Biomed. 192 (2020), 105442, https://doi.org/10.1016/j.cmpb.2020.105442.

[8] M.C. Paul, M. Mamun Molla, G. Roditi, Large-Eddy simulation of pulsatile blood flow, Med. Eng. Phys. 31 (2009) 153–159, https://doi.org/10.1016/j.medengphy.2008.04.014.

[9] M. Kiran Raj, S. Dasgupta, S. Chakraborty, Biomimetic pulsatile flows through flexible microfluidic conduits, Biomicrofluidics 13 (2019), https://doi.org/10.1063/1.5065901.

[10] B. Dincau, E. Dressaire, A. Sauret, Pulsatile Flow in Microfluidic Systems, Small 16 (2020) 1–18, https://doi.org/10.1002/smll.201904032.

[11] S. Gupta, S.A. Patel, R.P. Chhabra, Pulsatile flow of power-law fluids over a heated cylinder: Flow and heat transfer characteristics, Int. J. Therm. Sci. 152 (2020), 106330, https://doi.org/10.1016/j.ijthermalsci.2020.106330.

[12] U. Akdag, S. Akcay, D. Demiral, Heat transfer enhancement with laminar pulsating nanofluid flow in a wavy channel, Int. Commun. Heat Mass Transfer 59 (2014) 17–23, https://doi.org/10.1016/j.icheatmasstransfer.2014.10.008.

[13] E. Aslan, M. Ozsaban, G. Ozcelik, H.R. Guven, Numerical investigation for convective heat transfer and friction factor under pulsating flow conditions, MATEC Web of Conferences. 240 (2018) 1449–1457, https://doi.org/10.1051/matecconf/201824001003.

[14] F. Zhang, Y. Bian, Y. Liu, J. Pan, Y. Yang, H. Arima, Experimental and numerical analysis of heat transfer enhancement and flow characteristics in grooved channel for pulsatile flow, Int. J. Heat Mass Transf. 141 (2019) 1168–1180, https://doi.org/10.1016/j.ijheatmasstransfer.2019.06.100.

[15] H. Huang, Y. Bian, Y. Liu, F. Zhang, H. Arima, Y. Ikegami, Numerical and experimental analysis of heat transfer enhancement and pressure drop characteristics of laminar pulsatile flow in grooved channel with different groove lengths, Appl. Therm. Eng. 137 (2018) 632–643, https://doi.org/10.1016/j.applthermaleng.2018.04.013.

[16] F. Selimefendigil, Numerical analysis of mixed convection in pulsating flow for a horizontal channel with a cavity heated from below, Therm. Sci. 20 (2016) 35–44, https://doi.org/10.2298/TSCI120413137S.

[17] M. MdMolla, M.C. Paul, Large eddy simulation of pulsatile flow through a channel with double constriction, Fluids. 2 (2017), https://doi.org/10.3390/fluids2010001.

[18] D. Park, H. Shim, Y. Lee, PIV Measurement of Separation Bubble on an Airfoil at Low Reynolds Numbers, J. Aerosp. Eng. 33 (2020) 1–17, https://doi.org/10.1061/(ASCE)AS.1943-5525.0001099.

[19] *A. Khair, A. Hossain, B.C. Wang, D. Kuhn, M. Molla, Direct numerical simulation of physiological pulsatile flow through a stenotic channel, Proceedings of the International Symposium on Turbulence, Heat and Mass Transfer. 2012-Septe (2012) 1226–1238. 10.1615/ICHMT.2012.ProcSevIntSympTurbHeatTransfPal.1270.*

[20] T. Chavan, M. Chakraborty, A. Vaidyanathan, Experimental and modal decomposition studies on cavities in supersonic flow, Exp. Therm Fluid Sci. 135 (2022), 110600, https://doi.org/10.1016/j.expthermflusci.2022.110600.

[21] A.A. Bhuiyan, M.R. Karim, J.T. Hart, M.M. Rahman, J. Naser, Experimental and numerical investigation of coherent structure dynamics on mass transfer in a separated cavity flow, Exp. Therm Fluid Sci. 76 (2016) 146–162, https://doi.org/10.1016/j.expthermflusci.2016.03.028.

[22] K.M. Chung, K.H. Lee, K.C. Chang, Characteristics of cylindrical cavities in a compressible turbulent flow, Aerosp. Sci. Technol. 66 (2017) 160–164, https://doi.org/10.1016/j.ast.2017.03.022.

[23] S.L.N. Desikan, S. Pandian, P.P. Simha, N. Sahoo, Experiments on flow past cavity and the application of modal decomposition techniques, European Journal of Mechanics, B/fluids. 94 (2022) 293–298, https://doi.org/10.1016/j.euromechflu.2022.03.009.

[24] R. Fishler, M.K. Mulligan, J. Sznitman, Mapping low-Reynolds-number microcavity flows using microfluidic screening devices, Microfluid Nanofluidics. 15 (2013) 491–500, https://doi.org/10.1007/s10404-013-1166-0.

[25] T.M. Faure, L. Pastur, F. Lusseyran, Y. Fraigneau, D. Bisch, Three-dimensional centrifugal instabilities development inside a parallelepipedic open cavity of various shape, Exp. Fluids 47 (2009) 395–410, https://doi.org/10.1007/s00348-009-0671-0.

[26] G. Guo, Q. Luo, Flowfield structure characteristics of the hypersonic flow over a cavity: From the continuum to the transition flow regimes, Acta Astronaut. 161 (2019) 87–100, https://doi.org/10.1016/j.actaastro.2019.05.023.

[27] J. Zhang, E. Morishita, T. Okunuki, H. Itoh, Experimental investigation on the mechanism of flow-type changes in supersonic cavity flows, Trans Jpn Soc Aeronaut Space Sci. 45 (2002) 170–179, https://doi.org/10.2322/tjsass.45.170.

[28] P. Vilkinis, N. Pedišius, Analysis of reattachment length dynamics in cavities, Exp. Therm Fluid Sci. 119 (2020), https://doi.org/10.1016/j.expthermflusci.2020.110211.

[29] J. Henderson, K. Badcock, B.E. Richards, Subsonic and transonic transitional cavity flows, 6th Aeroacoustics Conference and Exhibit. (2000), https://doi.org/10.2514/6.2000-1966.

[30] S.E. Coleman, V.I. Nikora, S. r. McLean, E. Schlicke, Spatial averaged turbulent flow over square ribs, J Eng Mech. 133 (2007) 194–204. 10.1061/(ASCE)0733-9399(2007)133.
[31] S. Leonardi, P. Orlandi, R.J. Smalley, L. Djenidi, R.A. Antonia, Direct numerical simulations of turbulent channel flow with transverse square bars on one wall, J. Fluid Mech. 491 (2003) 229–238, https://doi.org/10.1017/S0022112003005500.
[32] Y. Zhang, B. Eichholz, R. Zhang, Evolution of vortex structures in an open deep cavity under pulsatile flow conditions: An experimental study, Phys. Fluids 34 (2022), https://doi.org/10.1063/5.0111653.
[33] S.S. Dol, M.M. Salek, R.J. Martinuzzi, Effects of Pulsation to the Mean Field and Vortex Development in a Backward-Facing Step Flow, J. Fluids Eng. 136 (2014) 2–7, https://doi.org/10.1115/1.4025608.
[34] A. Velazquez, J.R. Arias, J.L. Montanes, Pulsating flow and convective heat transfer in a cavity with inlet and outlet sections, Int. J. Heat Mass Transf. 52 (2009) 647–654, https://doi.org/10.1016/j.ijheatmasstransfer.2008.07.020.
[35] J. Šereika, P. Vilkinis, N. Pedišius, Investigation of pulsatile flow structure in closed-type cavity, Int. J. Heat Fluid Flow 92 (2021), https://doi.org/10.1016/j.ijheatfluidflow.2021.108877.
[36] A.S. Kherbeet, H.A. Mohammed, K.M. Munisamy, B.H. Salman, The effect of step height of microscale backward-facing step on mixed convection nanofluid flow and heat transfer characteristics, Int. J. Heat Mass Transf. 68 (2014) 554–566, https://doi.org/10.1016/j.ijheatmasstransfer.2013.09.050.
[37] J. Tihon, V. Pěnkavová, M. Pantzali, The effect of inlet pulsations on the backward-facing step flow, Eur. J. Mech. B. Fluids 29 (2010) 224–235, https://doi.org/10.1016/j.euromechflu.2010.02.001.
[38] J. Tihon, V. Pěnkavová, J. Havlica, M. Šimčík, The transitional backward-facing step flow in a water channel with variable expansion geometry, Exp. Therm Fluid Sci. 40 (2012) 112–125, https://doi.org/10.1016/j.expthermflusci.2012.02.006.
[39] K.B. Chun, H.J. Sung, Control of turbulent separated flow over a backward-facing step by local forcing, Exp. Fluids 21 (1996) 417–426, https://doi.org/10.1007/BF00189044.
[40] B.F. Armaly, F. Durst, J.C.F. Pereira, B. Schönung, Experimental and theoretical investigation of backward-facing step flow, J. Fluid Mech. 127 (1983) 473, https://doi.org/10.1017/S0022112083002839.
[41] G. Biswas, M. Breuer, F. Durst, Backward-facing step flows for various expansion ratios at low and moderate reynolds numbers, Journal of Fluids Engineering, Transactions of the ASME. 126 (2004) 362–374, https://doi.org/10.1115/1.1760532.
[42] *G. Ceglia, M. Invigorito, M. Chiatto, C.S. Greco, G. Cardone, L. De Luca, Flow control on a 2D back-facing ramp by Synthetic Jets, (2020) 294–298. 10.1109/metroaerospace48742.2020.9160104.*
[43] M. Chiatto, D. Hlevca, F. Grasso, L. de Luca, Modal Analysis of Actively Controlled Flow past a Backward Facing Ramp (2020), https://doi.org/10.2514/6.2020-0100.
[44] A. Kourta, A. Thacker, R. Joussot, Analysis and characterization of ramp flow separation, Exp. Fluids 56 (2015) 1–14, https://doi.org/10.1007/s00348-015-1968-9.
[45] A. Mushyam, J.M. Bergada, C. Navid Nayeri, A numerical investigation of laminar flow over a backward facing inclined step, Meccanica 51 (2016) 1739–1762, https://doi.org/10.1007/s11012-015-0335-5.
[46] M.M. Salek, S.S. Dol, R.J. Martinuzzi, Analysis of Pulsatile Flow in a Separated Flow Region, in, in: ASME 2009 Fluids Engineering Division Summer Meeting, 2009, pp. 1429–1438, https://doi.org/10.1115/FEDSM2009-78302.
[47] K. Ghorbanian, M.R. Soltani, M.D. Manshadi, Experimental investigation on turbulence intensity reduction in subsonic wind tunnels, Aerosp. Sci. Technol. 15 (2011) 137–147, https://doi.org/10.1016/j.ast.2010.06.009.